Chemical Engineering Journal 166 (2011) 368–377

Contents lists available at ScienceDirect

Chemical Engineering Journal

journal homepage: www.elsevier.com/locate/cej

Isobutane dehydrogenation in a DD3R zeolite membrane reactor

Johan van den Bergh*, Canan Gücüyener[1], Jorge Gascon[1], Freek Kapteijn*

Catalysis Engineering, ChemE, Delft University of Technology, Julianalaan 136, 2628 BL Delft, The Netherlands

ARTICLE INFO

Article history:
Received 7 June 2010
Received in revised form 2 November 2010
Accepted 5 November 2010

Keywords:
Zeolite membrane
Zeolite DD3R
Membrane reactor
Isobutane dehydrogenation
Chromia catalyst
Characteristic times

ABSTRACT

Dehydrogenation of isobutane has been studied in a DD3R zeolite membrane reactor (MR) at 712 and 762 K, using pure isobutane at 101 kPa as feed gas and N_2 as sweep gas. Clear advantage of using the small-pore zeolite DD3R is that it offers an absolute separation of H_2 from isobutane by a molecular sieving mechanism. Experiments in a conventional packed bed reactor served as benchmark. Cr_2O_3 on Al_2O_3 was used as catalyst.

The DD3R membrane showed an excellent H_2/isobutane permselectivity (>500 @ 773 K) and a reasonable H_2 permeance ($\sim 4.5 \times 10^{-8}$ mol m^{-2} s^{-1} Pa). At low residence times isobutene yields 50% above the equilibrium could be obtained. At 762 K and 0.13 kg_{feed} kg_{cat}^{-1} h^{-1}, the isobutene yield in the membrane reactor (MR) is 0.41, where the equilibrium yield is ~0.28. The increased performance is attributed to removal of H_2 from the reaction zone by the membrane, up to 85% at the lowest space velocity. The removal of H_2 mildly promotes coke formation, suppresses hydrogenolysis reactions and appears to slightly reduce the catalyst activity. The membrane permeation parameters and reaction rate constants have been estimated independently from membrane permeation and packed bed reactor (PBR) experiments, respectively. From these parameters the behaviour of the MR can be simulated well. Two important dimensionless parameters determine the MR performance primarily, the Damköhler (Da) and membrane Péclet number (Pe_δ). For a significant improvement of the MR performance as compared to a PBR $Da \geq 10$ and $Pe_\delta \leq 0.1$. $DaPe_\delta$ should be ≈1 to optimally utilize both catalyst and membrane. In the current MR unit both the hydrogen removal capacity and catalyst activity stand in the way of successful application. Using a more active catalyst *and* a more favourable area to volume ratio could greatly improve the MR performance. Operation at a higher feed pressure could be a possible solution. Since membranes with higher fluxes are already available, the limited catalyst activity and stability under relative low temperature and H_2 lean conditions are the important limiting factors regarding application of MRs in dehydrogenation reactions.

1. Introduction

Alkane dehydrogenation reactions are industrially very relevant, but they are also a class of reactions where the conversion can be (severely) equilibrium-limited at practical conditions [1]. Low conversions lead to a large flow of alkane/alkene mixtures that needs to be separated and recycled. Particularly the separation of alkanes/alkenes is very energy intensive [2]. An approach to increase the single-pass conversion is by using a membrane reactor (MR). By *in situ* removal of the product H_2 an apparent equilibrium shift can be accomplished. Moreover, if the equilibrium conversion based on the feed conditions does not limit the single pass conversion, the operating temperature could be decreased and pure H_2 can be obtained. An additional advantage of a lower operating temperature could be suppression of coke formation [3]. Clearly, the membrane should be suitable in terms of H_2 to hydrocarbon selectivity, H_2 permeance and stability. Therefore, many types of membranes [4] have been investigated for this type of application. For example, isobutane dehydrogenation has been studied using γ-alumina [5], zeolite MFI [5–9], Pd/Ag [10–12], Pd [9,13], dense silica [14] and carbon molecular sieve [15] membranes. Comparison of the achieved improvements of the different MR is difficult, since the operating conditions vary considerably. However, the general outcome is that in all cases a conversion above the equilibrium conversion could be obtained due to H_2 removal by the membrane. Eventually, the flux, selectivity, stability and price of the membrane will determine the viability of each type of MR. For several types of membranes the H_2/hydrocarbon selectivity and H_2 permeance are compared in Table 1. It is clear that Pd-based membranes stand out because they combine a very high H_2 selectivity with a high H_2 permeance. But, palladium membranes are relatively expensive, simply due to the high palladium price [8], and may be unstable

* Corresponding authors. Fax: +31 15 2785006.
E-mail addresses: j.vandenbergh@tudelft.nl (J. van den Bergh), f.kapteijn@tudelft.nl (F. Kapteijn).
[1] Fax: +31 15 2785006.

1385-8947/$ – see front matter © 2010 Elsevier B.V. All rights reserved.
doi:10.1016/j.cej.2010.11.021

Table 1
H_2 permeance and selectivity of various membranes used in the isobutane dehydrogenation reaction.

Membrane	Thickness (μm)	Pore size (nm)	H_2 permeance (10^{-7} mol m^{-2} s^{-1} Pa^{-1})	Selectivity (H_2/isobutane)	Reference
γ-Alumina	3	3	160 (723 K)	4 (723 K)[a]	[5]
Zeolite MFI	n.a.[b]	0.55	11 (723 K)	30 (723 K)[a]	[5]
Zeolite MFI	60	0.55	1.1 (773 K)	70 (773)[c]	[8]
Zeolite MFI	n.a.[b]	0.55	5 (~725 K)	10 (~725 K)[c]	[9]
Dense silica	0.1	n.a.[b]	0.2 (773 K)	80–300[a]	[14]
PdAg	10	Dense	9	1200 (H_2/N_2)	[10]
PdAg	6	Dense	40 (723 K)	Infinite	[12]
Pd	5	Dense	30 (~725 K)	60 (~725 K)[a]	[9]
DD3R	1–2	0.38 × 0.44	0.45 (773 K)	>500 (773 K)[a]	[25]

[a] Permselectivity.
[b] Information not available.
[c] Mixture selectivity.

[16]. Although zeolite membranes are also quite expensive [17], they could be more advantageous in terms of stability. However, the currently studied medium-pore zeolite MFI has pores larger than both isobutane and H_2, which leads to only a modest separation factor. Although infinite selectivity is not essential to obtain an improved reactor performance, the amount of hydrocarbons retained in the feed does determine the maximum level of conversion increase that can be obtained [18] and an infinite H_2 to hydrocarbon selectivity has the clear advantage of obtaining a pure H_2 flow at the sweep side of the reactor. Moreover, in case of relative large pores not only reactant loss is an issue, but also a significant dilution of the feed gas by counter-permeation of the sweep gas can occur [5,8]. This can be prevented, or at least minimized, by choosing a smaller-pore membrane that combines the stability of a zeolite membrane with the absolute H_2/isobutane selectivity found for Pd-based membranes. A zeolite MR with such properties could be much more viable compared to the zeolites studied so far.

An example of such a zeolite is DD3R which consists of cages connected by 8-ring window openings of 0.36 nm × 0.44 nm. This type of zeolite has received considerable attention in recent years: DD3R has been demonstrated to be very successful in propane/propene [19,20], CO_2/CH_4 [21–23] and water/ethanol [24] separations. Recently, we have demonstrated that this membrane shows a very high H_2/isobutane selectivity (>500, Table 1), which is maintained up to high temperatures [25].

The aim of this paper is to demonstrate and evaluate the performance of a DD3R zeolite membrane in dehydrogenation using the catalytic dehydrogenation of isobutane in a packed bed membrane reactor configuration as a model example. First, the permeation and separation properties of the membrane are discussed. Then the MR is evaluated in terms of isobutene yield, selectivity, catalyst activity and stability. Experiments in a conventional packed bed reactor are used as a benchmark for the MR results. A detailed model of the MR is used to support interpretation of the results. Finally, an analysis is made on the controlling processes in the MR performance by a characteristic times evaluation.

2. Experimental

2.1. Membrane experiments

Membrane permeation experiments were carried out using a tubular DD3R zeolite membrane provided by NGK Insulators [26]. The membrane is similar to the one used by Kuhn et al. [24]. A ~1–2 μm thick zeolite layer is present on the outside of a 150 mm long α-alumina tube. The outer diameter of the tube is 12 mm. The support consists of three layers of different pore size (0.2, 1 and 5 μm) and thickness (13, 70 and 1750 μm, respectively). The composite membrane was sealed in a stainless-steel module using graphite O-rings leaving 120 mm effective tube length and 0.0045 m^2 membrane area (Fig. 1). The inner diameter of the shell is 40 mm. Although the membrane tube is closed at one end, counter current plug-flow-like operation is obtained by feeding the gas from the closed end through a feed tube sticking inside the membrane tube as shown in Fig. 1. Single component permeation of H_2, and isobutane equimolar binary mixture permeation of H_2/isobutane mixtures were studied using nitrogen as sweep gas. Single component He permeances were measured in the pressure drop mode (no sweep gas). The permeate pressure was always at atmospheric pressure. The feed pressure was 101 kPa in case of the experiments with sweep gas and 200 kPa in case of pressure drop experiments, the temperature was varied between 303 and 773 K. In case of the He and H_2 single component experiments both the feed and sweep gas flow rate were set to 200 ml min^{-1} (STP). The experiments involving isobutane were performed at a feed and sweep gas flow rate of 100 ml min^{-1} (STP). All experiments were carried out in counter current mode. The retentate and permeate flows were determined using a soap film meter. The compositions of both flows were determined by GC analysis. In the case of isobutane a FID detector and for all other components a TCD detector was used. For H_2 detection Ar was used as carrier gas.

2.2. (Membrane) reactor experiments

The same membrane used for the permeation studies has been used in the membrane reactor (MR) experiments. The effective tube length available for permeation was 95 mm. Now the tube is packed with 4.1 g of chromia–alumina catalyst (Cr_2O_3/Al_2O_3), Harshaw (nowadays BASF Nederland) Cr-0211-T, 5/32″ (Cr_2O_3, 18.0%; ZrO_2, 0.25%; Al_2O_3, 82.0%). The catalyst was crushed and sieved to obtain particles with a diameter between 0.7 and 1.0 mm. The tube is packed with catalyst over the length of the permeable membrane area. Quartz wool was placed before and after the catalyst

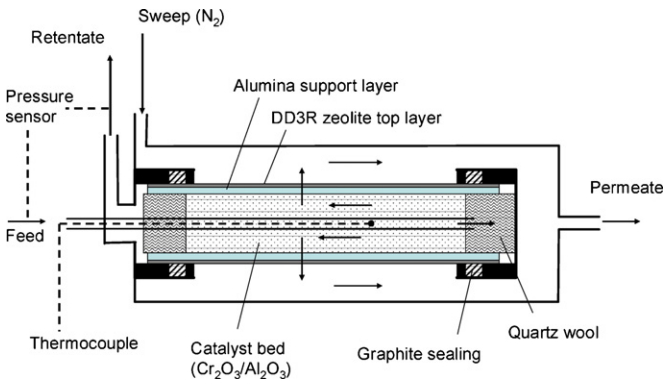

Fig. 1. Schematic drawing of the membrane reactor module. Arrows indicate the flow directions in the module.

bed. The temperature was measured in the feed tube that sticks through the catalyst bed. The pressure was measured before and after the packed bed. Pure isobutane at 101 kPa was fed in the range of 3.7–57 ml min^{-1} (STP) at 762 and 712 K with a counter current N_2 sweep gas flow rate of 100 ml min^{-1} (STP) at 101 kPa. The catalyst was regenerated overnight at the reaction temperature under a 2% O_2 in N_2 flow. The retentate and permeate flows and compositions are measured as described in Section 2.1.

As a benchmark for the membrane reactor results, experiments with an impermeable stainless-steel tube in the module instead of the DD3R membrane were performed. The same flow rates and catalyst loading as in case of the membrane were used. These experiments are referred to as packed bed reactor (PBR) experiments.

The isobutene yield (Y_E) is normally defined based on the in and outgoing molar flow rates (F) of isobutane (A) and isobutene (E):

$$Y_E = \frac{F_E^{out}}{F_A^{in}}. \tag{1}$$

However, this requires a very accurate estimate of the in and outgoing volumetric flow rates which appears difficult, particularly at low Weight Hourly Space Velocity (*WHSV*). Therefore, the yield is calculated based on merely the outgoing flows and compositions (x) according to:

$$Y_E = \frac{F_{tot}^{perm} x_E^{perm} + F_{tot}^{ret} x_E^{ret}}{F_{tot}^{perm} \sum_{i=1}^{4} \frac{i}{4}(x_{Ci}^{perm}) + F_{tot}^{ret} \sum_{i=1}^{4} \frac{i}{4}(x_{Ci}^{perm})}. \tag{2}$$

Here subscript *Ci* represents the different hydrocarbons grouped according to their carbon number: C1 (methane), C2 (ethane and ethane), etc. Also in this calculation procedure determination of the volumetric flows play a role, but since the amount of hydrocarbons in the permeate flow is very low, the influence of the flow rates on the estimated yield is minimal. By considering only the outgoing flows the formation of coke is neglected.

The conversion of isobutane is defined in a similar way:

$$X = 1 - \frac{F_{tot}^{perm} x_A^{perm} + F_{tot}^{ret} x_A^{ret}}{F_{tot}^{perm} \sum_{i=1}^{4} \frac{i}{4}(x_{Ci}^{perm}) + F_{tot}^{ret} \sum_{i=1}^{4} \frac{i}{4}(x_{Ci}^{ret})} \tag{3}$$

and the selectivity (S) towards isobutene as:

$$S_E = \frac{Y_E}{X}. \tag{4}$$

2.3. Membrane reactor modelling

For a quantitative interpretation of the membrane reactor results a model has been set up [4,27]. In the formulation of the model equations dimensionless numbers are introduced that characterize the MR's performance. The model includes convection and diffusion at the membrane tube and shell side, exchange of moles between the shell and tube side via the membrane and reaction in the catalyst bed held in the tube (Fig. 2). Radial dispersion, pressure drop over the packed bed and temperature gradients are neglected. The latter two assumptions have been validated by pressure and temperature measurements.

Let us now consider the above mentioned transport phenomena separately. The diffusive flux (N_i^{diff}) of component i in the shell and tube side is represented by Fick's law:

$$N_i^{diff} = -D_i^{g,eff} \frac{dc_i}{dx}, \tag{5}$$

where now an effective gas diffusion coefficient $D_i^{g,eff}$, concentration c and space x is found. The convective flux of each component at the shell and tube side is given by the product of the gas velocity (u) and its concentration:

$$N_i^{conv} = uc_i. \tag{6}$$

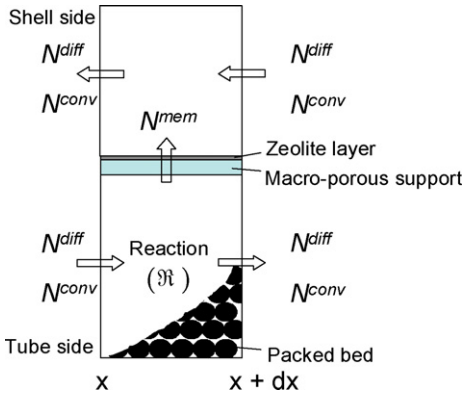

Fig. 2. Schematic representation of the MR and all processes that are considered in the model: Convection (*conv*) and diffusion (*diff*) in the shell and tube side, reaction in the tube and exchange of molecule across the membrane (*mem*) between the shell and tube side. All mass transport processes are indicated as fluxes (N).

The flux through the membrane is assumed to be determined completely by the zeolite layer; mass transport resistance in the support is neglected. Following earlier analysis of the membrane permeation data [25] it is assumed that isobutane flux through the membrane is only due to Knudsen diffusion through membrane defects. Mathematically this flux can be expressed as:

$$N_i^{mem} = \frac{D_{Kn,i}^{eff}}{\delta^{mem}} \frac{(p_i^T - p_i^S)}{RT}, \qquad D_{Kn,i}^{eff} = \frac{\varepsilon}{\tau} \frac{d_0}{3} \sqrt{\frac{8RT}{\pi M_i}} \tag{7}$$

where p, M, δ^{mem}, ε, τ and d_0 represent the pressure, molar mass, membrane thickness, membrane defect porosity, tortuosity and pore size, respectively. The superscripts S and T refer to shell and tube side properties, respectively. Also viscous flow plays a role [25], but this contribution can be neglected because in the current case only situations without an absolute pressure drop over the membrane are considered. The unknown properties in Eq. (7) are lumped:

$$\frac{\varepsilon}{\tau} \frac{d_0}{\delta^{mem}} \tag{8}$$

and have been fitted to the isobutane permeation data. The diffusivity of isobutene is based on the isobutane diffusivity corrected for the molar mass dependency expected from the Knudsen diffusion mechanism (Eq. (7)). The permeation data of N_2 and H_2 are assumed to follow a surface diffusion mechanism [25,28]. In case that mass transport occurs in a very weak adsorption regime the flux across the membrane can be expressed as:

$$N_i^{mem} = \frac{q_i^{sat} \rho}{\delta^{mem}} Đ_i K_i (p_i^T - p_i^S). \tag{9}$$

q^{sat} is the maximum loading in the zeolite and ρ the zeolite density. The Maxwell–Stefan *diffusivity* ($Đ$) and adsorption equilibrium constant (K) have the following temperature dependency:

$$K_i = K_{0,i} \exp\left(\frac{-\Delta H_{ads,i}}{RT}\right), \qquad Đ_i = Đ_{0,i} \cdot \exp\left(\frac{-E_{A,diff,i}}{RT}\right). \tag{10}$$

This yields the pre-exponential of the adsorption equilibrium constant (K_0), enthalpy of adsorption (ΔH_{ads}), the pre-exponential of the Maxwell–Stefan diffusivity ($Đ_0$) and the activation energy of the diffusivity ($E_{A,diff}$).

Eq. (9) can also be presented in a slightly different form, which is more convenient when expressing the equations in a dimensionless

form later on:

$$N_i^{mem} = \frac{D_i^{mem}}{\delta^{mem}}\frac{(p_i^T - p_i^S)}{RT}, \qquad \frac{D_i^{mem}}{\delta^{mem}} = RT\frac{\rho q_i^{sat} K_{0,i} Đ_{0,i}}{\delta^{mem}}\exp\left(\frac{-E_{A,i}^{app}}{RT}\right). \tag{11}$$

The apparent activation energy for diffusion is defined as:

$$E_A^{app} = E_{A,diff} + \Delta H_{ads}. \tag{12}$$

The lumped parameter $\rho q_i^{sat} K_{0,i} Đ_{0,i} (\delta^{mem})^{-1}$ and E_A^{app} have been estimated from the H_2 and N_2 permeation data. Note that Eq. (11) is also valid to predict the permeance in a mixture since the single component and mixture permeances are the same for the considered mixtures at high temperatures across the DD3R membrane [25].

The reaction rate in the packed bed is described by a Langmuir Hinshelwood type rate equation [29], assuming that isobutane adsorption is the rate-limiting step:

$$\Re\left[\frac{\text{mol}}{\text{kg}_{\text{cat}}\,\text{s}}\right] = \frac{k p_A (1 - (p_E p_H / p_A K_{eq}))}{1 + (p_E/K_E) + (p_H/K_H)}. \tag{13}$$

Here we can distinguish the partial pressures and adsorption equilibrium constants (K_i) of isobutane ($i = A$), isobutene (E) and hydrogen (H). K_{eq} represents the overall reaction equilibrium constant.

A molar balance for each component over a slice dz in axial direction ($z = x/L_{tube}$, L_{tube} = permeable tube length) of the isobaric membrane reactor tube side (Fig. 2) leads to:

$$0 = \frac{\pi d_{tube}^2}{4}\left(\frac{p_{tot}^T}{RT}\right)\frac{\delta x_i^T u^T}{\delta z} - \frac{\pi d_{tube}^2}{4}\left(\frac{p_{tot}^T}{RT}\right)\frac{D_i^{g,eff}}{L_{tube}}\frac{d^2 x_i^T}{dz^2} - \nu_i \Re m_{cat} + L_{tube}\pi d_{tube}\frac{D_i^{mem}}{\delta_{mem}}\frac{1}{RT}(p_i^T - p_i^S). \tag{14}$$

And on the shell side:

$$0 = \frac{\pi(d_{shell}^2 - d_{tube}^2)}{4}\left(\frac{p_{tot}^S}{RT}\right)\frac{\delta x_i^S u^S}{\delta z} - \frac{\pi(d_{shell}^2 - d_{tube}^2)}{4}\left(\frac{p_{tot}^S}{RT}\right)\frac{D_i^{g,eff}}{L_{tube}}\frac{d^2 x_i^S}{dz^2} - L_{tube}\pi d_{tube}\frac{D_i^{mem}}{\delta_{mem}}\frac{1}{RT}(p_i^T - p_i^S). \tag{15}$$

Here m_{cat} and ν represent the catalyst mass and stoichiometric coefficient, respectively. Now we introduce a dimensionless gas velocity ϑ, a Péclet number relating the diffusive and convective flux in the packed bed (Pe_L), the Damköhler number (Da) and a Péclet number relating the convective flux in the packed bed and membrane flux (Pe_δ). Note that the Péclet numbers are based on the properties of H_2 since this characterizes the system best. Da is defined assuming first order kinetics in isobutane to arrive at a concentration independent dimensionless number:

$$\vartheta^T = \frac{u^T}{u_0^T}, \quad Pe_L^T = \frac{L_{tube}u_0^T}{D_H^{g,eff}}, \quad Da = \frac{4RTkm_{cat}}{u_0^T \pi d_{tube}^2}, \quad Pe_\delta^T = \frac{\delta^{mem}u_0^T}{4D_H^{mem}}\frac{d_{tube}}{L_{tube}}$$
$$\vartheta^S = \frac{u^S}{u_0^S}, \quad Pe_L^S = \frac{L_{tube}u_0^S}{D_H^{g,eff}}, \quad Pe_\delta^S = \frac{\delta^{mem}u_0^S}{4D_H^{mem}}\frac{(d_{shell} - d_{tube})}{L_{tube}}. \tag{16}$$

In addition to these dimensionless numbers the $DaPe_\delta$ number [30], a type of Damköhler number describing the ratio of reaction rate and membrane flux is defined:

$$DaPe_\delta = \frac{k\delta^{mem}d_{tube}}{D_H^{mem}}. \tag{17}$$

In the case the tube and shell side have the same total pressure Eq. (14) can be written as:

$$0 = x_i^T\frac{\delta\vartheta^T}{\delta z} + \vartheta^T\frac{\delta x_i^T}{\delta z} - \left(\frac{D_i^{g,eff,T}}{D_H^{g,eff,T}}\right)\frac{1}{Pe_L^T}\frac{d^2x_i^T}{dz^2} - \frac{\nu_i\Re}{p_{tot}^T k}Da + \left(\frac{D_i^{mem}}{D_H^{mem}}\right)\frac{1}{Pe_\delta^F}(x_i^T - x_i^S) \tag{18}$$

and Eq. (15) can be cast into:

$$0 = x_i^S\frac{\delta\vartheta^S}{\delta z} + \vartheta^S\frac{\delta x_i^S}{\delta z} - \left(\frac{D_i^{g,eff,S}}{D_H^{g,eff,S}}\right)\frac{1}{Pe_L^S}\frac{d^2x_i^S}{dz^2} - \left(\frac{D_i^{mem}}{D_H^{mem}}\right)\frac{1}{Pe_\delta^S}(x_i^T - x_i^S). \tag{19}$$

The final set of equations that constitutes the membrane reactor model comprises Eqs. (18) and (19) repeated for each component together with two equations that ensure that the sum of all fractions in the feed and sweep side equals 1:

$$1 = \sum_{i=1}^{n} x_i^T, \qquad 1 = \sum_{i=1}^{n} x_i^S. \tag{20}$$

This system of equations has been solved in Athena Visual Studio [31] as a boundary value problem using orthogonal collocation. The system is modelled as a closed system using Danckwerts type boundary conditions:

$z = 0$, tube side	$z = 1$, tube side
$x_{i,0}^T = x_i^T - \left(\frac{D_i^{g,eff,T}}{D_H^{g,eff,T}}\right)\frac{1}{Pe_L^T}\frac{dx_i^T}{dz}$	$\frac{dx_i^T}{dz} = 0$
$\vartheta^T = 1$	$\frac{d\vartheta^T}{dz} = 0$
$z = 0$, shell side	$z = 1$, shell side
$\frac{dx_i^S}{dz} = 0$	$x_{i,0}^S = x_i^S - \left(\frac{D_i^{g,eff,S}}{D_H^{g,eff,S}}\right)\frac{1}{Pe_L^S}\frac{dx_i^S}{dz}$
$\frac{d\vartheta^S}{dz} = 0$	$\vartheta^S = 1$

(21)

3. Results and discussion

3.1. Membrane permeation

The performance of the DD3R membrane up to 773 K has been studied previously [25]. The fluxes of He, N_2, H_2 and isobutane from this study are shown in Fig. 3. The fluxes of N_2 and H_2 have been modelled assuming that the mass transport across the membrane is governed by intra-crystalline surface diffusion (Eq. (11)), isobutane is modelled assuming permeation through defects by a Knudsen diffusion mechanism (Eq. (7)). More details on the models can be found in Section 2.3, while the permeation results have been discussed in detail in Ref. [25]. The model fit parameters that apply are listed in Table 2.

The isobutane flux is very low because it cannot enter the DDR pores and passes only through a small number of defects in the membrane. As compared to the medium-pore zeolite MFI, the H_2 permeance of DD3R is about one order of magnitude lower (Table 1). It appears that by reducing the pore size also the permeance is reduced.

Both the H_2 and isobutane flux show a slightly decreasing flux with increasing temperature. This leads to an almost constant ideal selectivity of more than 500 over the complete temperature range, as shown in Fig. 4. The ideal selectivity (α^{ideal}) is based on the single component permeances:

$$\alpha_{ij}^{ideal} = \frac{Permeance_i}{Permeance_j} = \frac{N_i^{mem}}{N_j^{mem}}\frac{(p_j^{retentate} - p_j^{sweep})}{(p_i^{retentate} - p_i^{sweep})}. \tag{22}$$

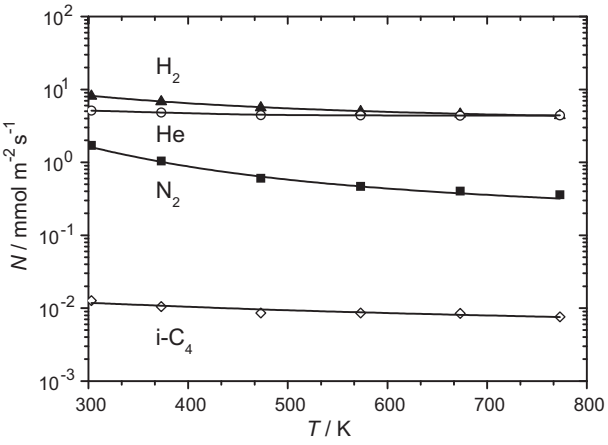

Fig. 3. Permeance of H_2, He, N_2 and isobutane through the DD3R membrane as a function of the temperature. The H_2 and N_2 data in the current study (closed symbols) represent counter-current permeation data using H_2 as feed and N_2 as sweep gas. The He permeances are measured using the pressure drop method with a pressure drop of 100 kPa. Isobutane is measured using a feed gas pressure of 101 kPa and sweep gas (N_2) pressure of 101 kPa. Lines represent model fit results, except in case of He where the drawn line is to guide the eye.

The mixture selectivity (α_{ij}^{mix}) is based on mixture permeation results and is defined as:

$$\alpha_{ij}^{mix} = \left(\frac{x_j}{x_i}\right)^{feed} \left(\frac{x_i}{x_j}\right)^{permeate} \quad (23)$$

The H_2/isobutane mixture selectivity is slightly lower than the ideal selectivity due to non-differential effects: the faster permeating H_2 reduces its driving force for permeation by increasing its partial pressure in the permeate and reducing its partial pressure in the feed side [25]. The H_2/isobutane selectivities also decrease slightly with increasing pressure due to a viscous flow contribution to the isobutane flux in case of an absolute pressure drop over the membrane. The H_2/N_2 (~11, 773 K) is much higher than the H_2/He (~1, 773 K) ideal selectivity. This makes N_2 the preferred choice as sweep gas in terms of minimal feed dilution by counter-permeation of the sweep gas.

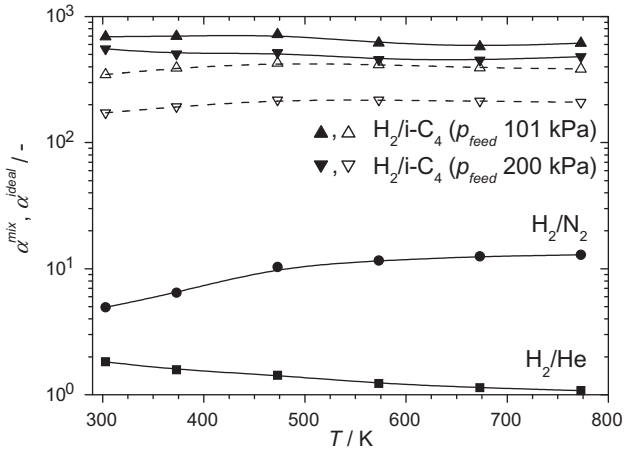

Fig. 4. Mixture and ideal selectivities of the DD3R membrane. Closed symbols and solid lines represent ideal selectivities, dashed lines and open symbols mixture selectivities under non-differential operation. The lines are added to guide the eye. All data are considered at a total pressure drop of 100 kPa over the membrane. In case of the H_2/isobutane mixture also the data at a feed pressure of 101 kPa without pressure drop over the membrane are shown.

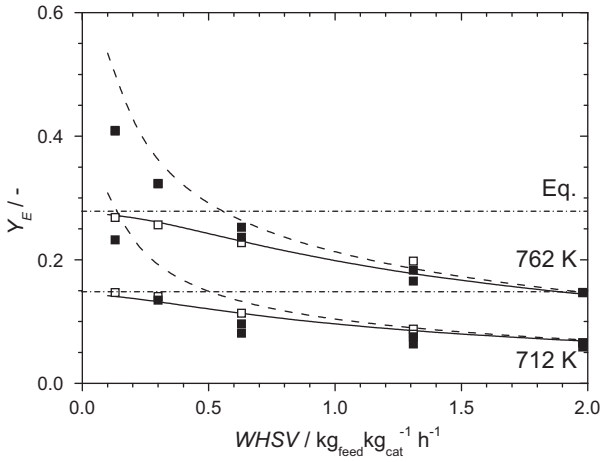

Fig. 5. Isobutene yield in a packed bed (open symbols) and membrane reactor (closed symbols) at 762 and 712 K as a function of the *WHSV*. Pure isobutane is fed at 101 kPa, N_2 is used as sweep gas in counter-current mode. Solid, dashed and dash-dot lines represent PBR model fit results, MR model predictions and the equilibrium conversion, respectively.

3.2. Packed bed (membrane) reactor

3.2.1. Asymmetry and packing effects

Compared to the membrane results in the previous section the membrane tube is filled with catalyst particles and the feed gases are fed from the inside of the tube (from the support side) instead of from the outside of the tube (from the zeolite layer side). If the support resistance can be ignored no difference in permeance should be observed if the gas is permeating from the support or from the zeolite layer side [32]. To ensure that the permeation data are suitable input to model the MR performance, an experiment has been performed with the packed bed membrane reactor at 303 K and 101 kPa using an equimolar H_2/isobutane mixture passing through the tube side and N_2 as sweep gas passing through the shell side. The H_2 and N_2 permeances are the same as in the membrane permeation experiments, while the isobutane permeance is a factor 2 lower.

3.2.2. Isobutene yield

Fig. 5 shows the isobutene yield in the PBR and MR at 762 and 712 K, together with model fit results of the PBR and model predictions of the MR. The MR and PBR have been modelled using the reactor model as described in Section 2.3, where in case of the PBR the membrane fluxes are set to zero. The gas phase diffusivities are predicted using the correlation of Fueller et al. [33], accounting for the packed bed porosity and tortuosity, which are assumed to be 0.4 and 1.5, respectively. The reaction rate kinetic constants have been estimated by model fitting of the packed bed yield data. The rate constants of Happel et al. [29] have been used as starting point because these have been determined on a similar catalyst (Cr_2O_3/Al_2O_3) in a suitable temperature range (650–762 K). The pre-exponential and activation energy of the rate constant have been estimated. Additionally, the pre-exponential of the reaction equilibrium constant has been fitted to reconcile the model and experimental equilibrium yields. The H_2 and isobutene adsorption equilibrium constants have been kept constant. The original constant values of Happel et al. and the model fit results of the current study are listed in Table 2. Note that the estimated values and the original ones of Happel et al. are in good agreement.

The PBR conversion data show an increase in yield with increasing temperature due to an increased catalysts activity and an increased equilibrium conversion. At low *WHSV*, *i.e.* long contact

Table 2
Estimated values from model fitting for membrane permeation and reaction rate parameters.

Membrane transport parameters		Units
Isobutane	$\frac{\varepsilon}{\tau}\frac{d_0}{\delta^{mem}} = 2.7 \times 10^{-9}$	
N_2	$D^{mem}(\delta^{mem})^{-1} = RT \cdot 1.12 \times 10^{-9} \exp\left(\frac{7000}{RT}\right)$	m s^{-1}
H_2	$D^{mem}(\delta^{mem})^{-1} = RT \cdot 2.88 \times 10^{-8} \exp\left(\frac{2880}{RT}\right)$	m s^{-1}
Reaction rate parameters		Units
Happel et al. [29]	Fitted parameters	
$k = 5.1 \times 10^{-03} \exp\left(-\frac{74822}{RT}\right)$	$k = 1.2 \times 10^{-03} \exp\left(-\frac{67509}{RT}\right)$	mol kg$_{cat}^{-1}$ s^{-1} Pa^{-1}
$K_{eq} = 1.4 \times 10^{+12} \exp\left(-\frac{121638}{RT}\right)$	$K_{eq} = 1.8 \times 10^{+12} \exp\left(-\frac{121638}{RT}\right)$	Pa^{-1}
$K_E = 2.1 \times 10^{-10} \exp\left(\frac{74822}{RT}\right)$	$K_E = 2.1 \times 10^{-10} \exp\left(\frac{74822}{RT}\right)$	Pa^{-1}
$K_H = 4.2 \times 10^{-12} \exp\left(\frac{100738}{RT}\right)$	$K_H = 4.2 \times 10^{-12} \exp\left(\frac{100738}{RT}\right)$	Pa^{-1}

times, the PBR yield approaches the equilibrium yield. The model fit results describe the PB data well.

The MR yields coincide with the PBR yields at high *WHSV* and at low *WHSV* the yields of the MR are significantly higher than the PBR and equilibrium yield. The MR model predictions are in fairly good agreement with the experimental MR data, but the yields appear to be slightly overpredicted. An explanation could be that the catalyst activity is decreased in case of the MR due to H_2 removal from the reaction zone, which is not accounted for in the current model. This effect has also been observed by Casanave et al. [6]. An indication of this behaviour can also be found from the comparison of the PBR and MR yield data at 712 K where the MR yield is slightly lower than the PBR yield, whereas model predictions always indicate a higher MR yield due to removal of H_2 from the reaction zone. However, the difference between the simulated and experimental yields could also be due to model assumptions like neglecting radial dispersion. Moreover, the conversion level for which the kinetic constants have been estimated does not match the level for which the prediction is made at low WHSV. The reduced activity could therefore also be due to inhibition by the product isobutene, which is underestimated in the rate equation. Airaksinen et al. [34] estimated for instance an isobutene adsorption equilibrium constant 8 times as high as the value we used in our study. But, by fitting the rate constant using a higher isobutene equilibrium adsorption constant from the PBR data does not lead to significantly different results.

The fraction of H_2 present in the retentate in case of the MR and PBR is shown in Fig. 6. This figure clearly illustrates that due to removal of H_2 from the reaction zone at low *WHSV* the MR outperforms the PBR. Whereas at high *WHSV* the membrane H_2 flux is not sufficient to remove a significant amount of H_2 and the MR and PBR performances are equal. It is also evident that the H_2 concentration reduction in the tube side of the MR compared to the PBR is that significant that if the catalyst activity is reduced when the hydrogen concentration is reduced this effect will become manifest at *WHSV* values < 1 h^{-1}.

Note that also at low *WHSV*s the hydrocarbon retention in the feed side is very high due to the excellent H_2/isobutane selectivity of the membrane. Even at a *WHSV* of 0.13 h^{-1} < 2% of the isobutane and isobutene leave the MR from the permeate side, >98% is retained in the feed side.

3.2.3. Selectivity

Besides isobutene also side products like coke or lower hydrocarbons can be formed. When coke is formed the amount of H_2 will be higher than the amount of isobutene in the reactor effluent. In case of the PBR experiments no excess of H_2 to isobutene could be detected. Although difficult to calculate accurately, there appears to be a significant excess of H_2 in case of the membrane reactor up to 10–15% at 762 K and low *WHSV*s. In case that for each mol isobutane converted to coke four mol of H_2 are formed and, accounting for the amount of H_2 consumed in the hydrogenolysis reactions, this leads to a selectivity towards coke of ~3% at *WHSV* = 0.13 h^{-1}. These results indicate that indeed due to H_2 removal coke formation is mildly promoted, particularly at long residence times.

The selectivity towards isobutene (Eqs. (4) and (2)) with respect to lower hydrocarbons in the MR is compared to the selectivity in the PBR at 712 and 762 K (Fig. 7). At high *WHSV* the selectivity is high, >0.96 for all cases. Upon increasing the residence time in the

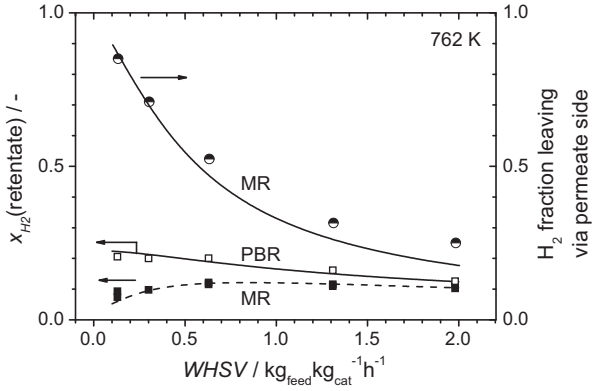

Fig. 6. Fraction of H_2 in the retentate of the PBR and MR at 762 K as a function of the *WHSV*. Points are experimental data, lines are modelling results.

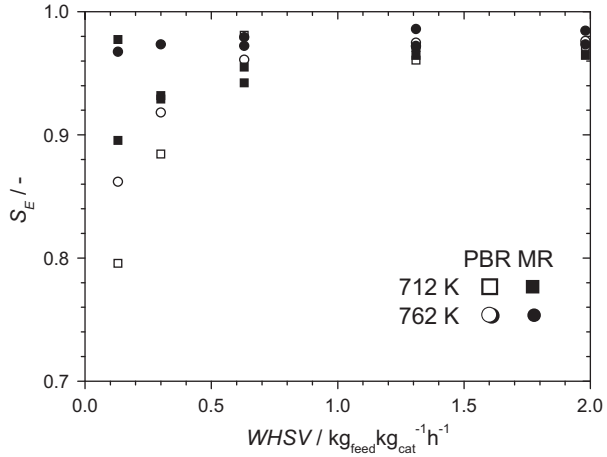

Fig. 7. Selectivity of the isobutane dehydrogenation reaction towards isobutene in the PBR and MR at 712 and 762 K as a function of the *WHSV*.

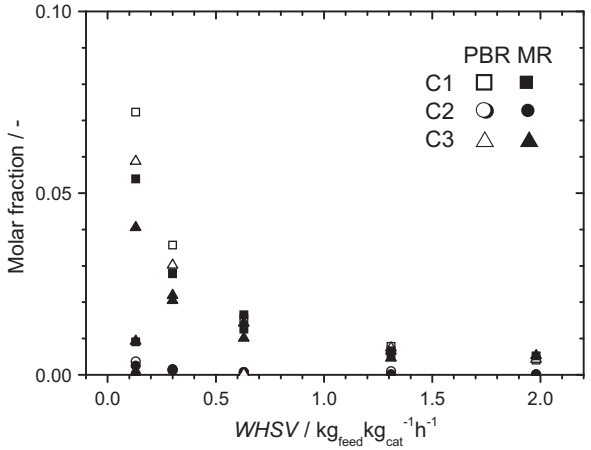

Fig. 8. Molar fraction of C1 (methane), C2 (ethane and ethane) and C3 (propane and propene) of all hydrocarbons that leave the MR and PBR at 762 K.

reactor more lower-hydrocarbons are formed. Also at higher temperature more by-products are formed. In all cases the major part of the by-products is constituted of methane and propane/propene (Fig. 8). Propane/propene and methane are present in almost equimolar amounts; only a modest excess of methane is present. This is expected since these are the products of hydrogenolysis of isobutane and isobutene. The amount ethane/ethene formed is very low. A comparison of the selectivity in the PBR and MR reveals that hydrogenolysis reactions are suppressed in the MR, most probably due to removal of H_2 from the reaction zone. This has also been found in other studies [10,13,14].

3.2.4. Catalyst and membrane stability

Although it appears that the catalyst activity in the MR is lower compared to the PBR (Section 3.2.2), no signs of very rapid catalyst deactivation in time have been observed. An experimental run at 762 K is shown in Fig. 9. Initially, a *WHSV* of 0.3 h^{-1} has been set. Note that at these conditions a significant amount of H_2 is removed from the reaction zone (Fig. 6) and that the conversion is above the equilibrium conversion (Fig. 9). Firstly, the catalyst shows a high activity, leading to a conversion of 0.4, then the conversion drops quickly, passes through a minimum and becomes constant after 2 h of operation. The initial high conversion is due to oxidation of part of the feed by the pre-oxidized catalyst.

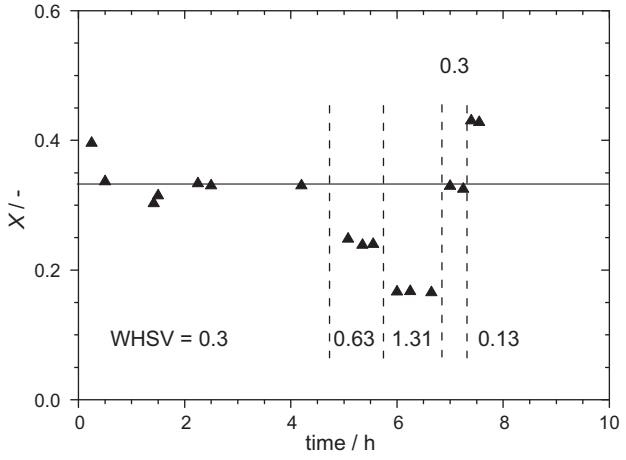

Fig. 9. Isobutane conversion as a function of time on stream in the MR at 762 K. During operation time the *WHSV* was changed from 0.3 to 0.63 to 1.31 to 0.3 and 0.13 h^{-1}.

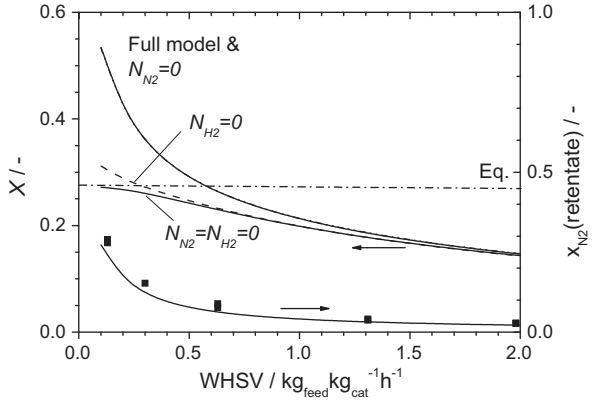

Fig. 10. Effect of feed dilution by counter-permeation of sweep gas on the membrane reactor conversion. Lines represent model simulations of the reactor reflecting the MR experiments (full model) and simulations assuming that the membrane is impermeable to the sweep gas ($N_{N_2} = 0$), impermeable to H_2 ($N_{H_2} = 0$) and impermeable to both H_2 and N_2 ($N_{H_2} = N_{N_2} = 0$). The right axis represents the fraction of N_2 in the retentate. The line represents simulation results of the full model, points are experimental data. The membrane reactor operates at 101 kPa pure isobutane feed, 762 K and 100 ml min^{-1} sweep gas (N_2) in counter-current mode.

Changing the *WHSV* leads to a new steady state conversion quickly. After 7 h of operation the steady state conversion at 0.3 h^{-1} after 2 h could be reproduced. Although the total number of turnovers is not very high, a stable MR operation without significant catalyst deactivation for several hours is observed under H_2 lean conditions.

Prior to the MR experiments the membrane has been exposed to high temperature conditions for the permeation experiments for several months (~6) including >10 temperature heating up and cooling down cycles [25]. The MR experiments added another 3 months of operation at high temperature (>700 K). Of this period ~25 working days of dehydrogenation experiments have been carried with the same number of overnight regenerations. In this period 5 heating up and cooling down cycles have been performed. The isobutane fraction in the permeate has been around 6×10^{-4} to 1×10^{-3} during all MR experiments. No significant increase of this fraction has been observed which indicates a stable membrane performance.

3.2.5. Feed dilution effects

In Section 3.2.2 the good performance of the MR has been attributed to the removal of H_2 from the reaction zone. Counter permeation of the sweep gas (N_2), however, can lead to dilution of the feed which can also contribute to an increased conversion [5,8] because the equilibrium conversion is higher at lower partial pressures. Fig. 10 shows the fraction of N_2 in the retentate due to counter permeation. Due to the longer residence time at the feed side the fraction of N_2 increases with decreasing *WHSV* up to almost 0.3 at a *WHSV* of 0.13 $kg_{feed}\ kg_{cat}^{-1}\ h^{-1}$. Note that this value represents the upper limit of the N_2 concentration in the tube.

To investigate the influence of the feed dilution on the yield, the MR conversion is simulated for several cases (Fig. 10): (1) experimental conditions: full model as considered in the previous sections, (2) no feed dilution: no N_2 flux across the membrane, (3) no H_2 flux across the membrane and (4) Completely impermeable membrane, *i.e.* a PBR. As shown previously (Fig. 5), the PBR approaches the equilibrium yield at low *WHSV* (Fig. 10). When no hydrogen is removed, but the feed is diluted due to N_2 counter permeation (case 3) the conversion becomes significantly higher than the equilibrium. Now a modest conversion increase due to dilution is found. The MR conversions with (case 1) and without (case 2) sweep gas counter permeation are exactly the same. Clearly the effect of feed dilution on the isobutene yield under experimen-

Table 3
Dimensionless numbers relating residence time and reaction time (Da), time to remove H_2 and residence time (Pe_δ), and time to remove H_2 and reaction time ($DaPe_\delta$).

WHSV	T (K)	Da	Pe_δ	$Da_L Pe_\delta$
0.1	762	5.31	0.12	0.63
0.3	762	1.77	0.36	0.63
1.0	762	0.53	1.19	0.63
0.1	712	2.54	0.12	0.29
0.3	712	0.85	0.35	0.29
1.0	712	0.25	1.16	0.29

tal conditions is minimal. The effect of feed dilution will only be of importance when the reactor operates close to the local thermodynamic equilibrium, which is not the case under the current conditions. The latter claim is verified by an evaluation of the retentate composition. The equilibrium constant and the reactant and product fractions are under equilibrium conditions related by:

$$K_{eq} = p_{tot}\left\{\frac{x_H x_E}{x_A}\right\}_{eq}. \quad (24)$$

The right hand side of the equation, evaluated for the retentate composition at 0.1 h^{-1} and 762 K, is 6351 Pa, which is about 1.5 times lower than the equilibrium value of 9320 Pa (left hand side).

3.2.6. Performance evaluation

The MR is evaluated further based on the dimensionless numbers introduced in Section 2.3. If we neglect axial and radial dispersion, three processes need to be balanced to obtain an optimal MR performance [17,35]. In terms of characteristic times these are: residence time, reaction time and a time related to hydrogen removal by the membrane. Combining these characteristic times leads to three different ratios: Da (residence time/reaction time), Pe_δ (time for H_2 removal/residence time) and $DaPe_\delta$ (time for H_2 removal/reaction time) (details in Section 2.3). The values of these dimensionless numbers for the MR are given in Table 3 at 762 and 712 K and different *WHSV*s. Da increases with increasing temperature due to the activated nature of the rate constant. At low *WHSV* the residence time is long compared to the reaction time and a high conversion is expected and obtained (Fig. 5). As a rule of thumb Da is related to the conversion as [36]: if $Da < 0.1$ then $X < 0.1$ and if $Da > 10$ then $X > 0.9$. Our results follow this rule of thumb well considering that our conversion scales from 0 to the equilibrium conversion. Pe_δ is almost independent of temperature because the membrane permeation of H_2 is only slightly dependent on the temperature (Fig. 3). At $WHSV = 1.0\ h^{-1}$ the residence time and time required for H_2 removal are of the same order ($Pe_\delta \approx 1$). This is illustrated nicely in Fig. 6, where indeed at this *WHSV* a considerable amount of H_2 is produced and removed from the reaction zone. Moving to lower *WHSV*s the residence time increases, whereas the characteristic time for H_2 removal remains constant, leading to an improved H_2 removal and reaction performance. Finally, $DaPe_\delta$ increases with increasing temperature since the characteristic time for reaction is reduced and the time for H_2 removal remains close to constant. The value of $DaPe_\delta$ is close to one, which indicates that in the current design the catalyst activity and membrane performance are balanced quite well. However, since the MR outperforms the PBR only at low *WHSV*s the appropriate conclusion is that both are not optimal regarding application of this MR. Note that compared to other type of MRs the H_2 permeance of the DD3R membrane is relatively low (Table 1). In those studies typically the catalyst activity is the factor limiting the MR performance [9,10,13].

To demonstrate that both the catalyst and membrane limit the performance, the MR is simulated considering the cases that: (1) Da is 10 times higher; (2) Pe_δ is 10 times lower and (3) that both Da is 10 times higher and Pe_δ is 10 times lower. The simulated conversions are compared to the original Da and Pe_δ values (Fig. 11).

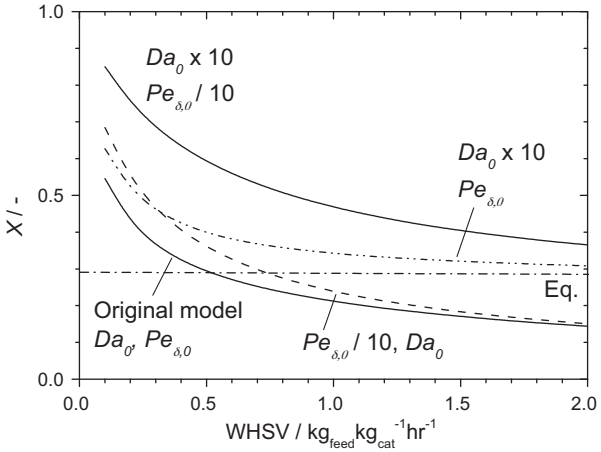

Fig. 11. Effect of variations of Da and Pe_δ on the MR conversion. Lines represent MR simulations at 762 K and 101 kPa total feed pressure, using 100 ml min^{-1} (STP) N_2 as sweep gas in countercurrent operation at 101 kPa. Starting from the original Da_0 and $Pe_{\delta,0}$ values simulations using a 10 times higher Da or a 10 times lower Pe_δ or a combination of the two have been performed.

Increasing the H_2 removal rate ($Pe_\delta \downarrow$) leads to a very modest conversion improvement, clearly the catalyst activity hampers an improved MR performance. If only the catalyst activity is increased ($Da\uparrow$), the reactor approaches its equilibrium conversion already at a much higher *WHSV*, but the membrane permeation flux is too low to obtain conversions significantly above the equilibrium at high *WHSV*s. If both the reaction activity and H_2 membrane removal rate are increased by a factor 10 ($Da\uparrow$ and $Pe_\delta \downarrow$), the conversion is strongly increased, as expected. Alternatively, the space velocity can be reduced by a factor 10, but then axial dispersion will become increasingly important with a negative impact on the plug flow reactor behaviour. For further reading on the influence on other operational aspects of MR in dehydrogenation reactions see for instance [18,37].

Several options could be applied to improve the MR's performance. Da can be increased by using a more active catalyst [38], or using a higher operating temperature (although a higher temperature would lead to a higher coking rate at the catalyst). A decrease of Pe_δ (Eq. (16)) can be achieved by removing more H_2 through application of a thinner DDR membrane, a different membrane with a higher permeance or by choosing a higher membrane area to reactor volume ratio. This latter area to volume ratio can be greatly increased by choosing a smaller tube or hollow fibrous support [35,39]. Note that Da can be increased and Pe_δ decreased efficiently by increasing the feed pressure since this will lead to a decreased gas velocity at a given *WHSV*, a higher reaction rate and a higher permeation flux. A potential downside of this approach can be that the increased hydrocarbon partial pressures could lead to a reduced catalyst selectivity or activity.

Note that van de Graaf et al. [35] have discussed their MR by comparing the membrane Areal Time Yield (ATY) and Space Time Yield (STY). In order to balance the two yields the area to volume ratio (A/V) can be changed. A clear connection between their and the present approach exists since:

$$DaPe_\delta \approx \frac{STY}{ATY}\frac{V}{A} = \frac{STY}{ATY}\frac{d_{tube}}{4}. \quad (25)$$

Another issue for application of this type of reactor is that it seems that removal of H_2 leads to a lower activity (Section 3.2.2) and more coke formation. As shown in Fig. 6 the H_2 fraction in the retentate needs to be strongly reduced to obtain high conversions. Since in this reaction only H_2 is removed and isobutene is retained, the H_2

fraction needs to be very low to achieve very high conversions due to the reaction equilibrium constant (*cf.* Eq. (24)).

The ultimate viability of the MR should be based on an economical evaluation and clear insights in the effects of very H_2 lean conditions on the catalyst performance. However, from the current results it can be concluded that the minimum requirements of a MR to obtain a significant conversion improvement compared to a PBR are: $Da \geq 10$ and $Pe_\delta \leq 0.1$, while $DaPe_\delta$ should be ≈ 1 to optimally utilize both catalyst and membrane activity.

Note that since membranes with higher fluxes are already available, it is the limited catalyst activity and stability under relative low temperature and H_2 lean conditions that is an important limiting factor regarding application of MRs in dehydrogenation reactions [38].

4. Conclusions

A DD3R zeolite membrane has been successfully applied as H_2 selective membrane in the dehydrogenation reaction of isobutane in a packed bed membrane reactor (MR) configuration. Experiments with a conventional packed bed reactor (PBR) serves as benchmark. The membrane shows an excellent H_2/isobutane permselectivity (>500 @ 773 K) and a reasonable H_2 permeance ($\sim 4.5 \times 10^{-8}$ mol m^{-2} s^{-1} Pa). The high selectivity is due to molecular sieving: isobutane cannot enter the pores of DD3R and passes only through membrane defects.

At low *WHSV*s isobutene yields above the equilibrium yield based on feed conditions could be obtained. At 762 K and 0.13 kg_{feed} kg_{cat}^{-1} h^{-1}, the isobutene yield in the MR is 0.41, where the equilibrium and PBR yields are only ~0.28, an increase of about 50%. This increased yield is attributed to removal of H_2 from the reaction zone by the membrane, up to 85% at the lowest space velocity. Although some counter permeation of the sweep gas N_2 occurs, this dilution effect does not contribute significantly to the yield increase of the MR. The activity of the catalyst in the MR seems modestly reduced compared to the PBR, but no indications of faster deactivation of the catalyst are observed under H_2 lean conditions. A constant very high hydrocarbon retention in the reaction zone indicated that the membrane quality remained constant throughout all experiments.

Compared to the PBR the selectivity in the MR towards coke seems to be mildly increased due to the lower H_2 partial pressure in the reactor, although the selectivity towards coke is still low: <5%. The selectivity towards methane and propane/propene is somewhat lower in the MR. By keeping the H_2 concentration in the reactor low, cracking hydrogenolysis reactions are mildly suppressed.

An isothermal membrane reactor model captures the experimental results well. The membrane permeation parameters and reaction rate constants have been estimated independently from membrane permeation and PBR experiments, respectively.

An analysis of the major characteristic times describing the system, the residence time in the reactor, reaction time and time required for H_2 removal by the membrane, expressed as ratios in two dimensionless parameters *Da* and Pe_δ, revealed that in the current MR design the catalyst activity and H_2 removal rate are nicely balanced ($DaPe_\delta \approx 1$), but both limit the overall performance. Improvements of the current design are possible by choosing a more active catalyst, or higher operating temperature, and a membrane support with a higher surface area per unit reactor volume. Also operation at higher feed pressure could boost the MR's performance. $Da \geq 10$ and $Pe_\delta \leq 0.1$ are proposed as minimal requirements of a MR to show a significantly improved performance compared to a PBR. $DaPe_\delta$ should be ≈ 1 to optimally utilize both catalyst and membrane activity. Since membranes with higher fluxes are already available, it is the limited catalyst activity and stability under relative low temperature and H_2 lean conditions that is an important limiting factor regarding application of MRs in dehydrogenation reactions [38].

Notation

A	area (m^2)
ATY	Areal Time Yield (mol m^{-2} s^{-1})
c	concentration (mol m^{-3})
d_0	membrane defect pore size (m)
d_{tube}	tube diameter (m)
D	diffusivity (m^2 s^{-1})
Da	Damköhler number, defined in Eq. (16)
$DaPe_\delta$	type of Damköhler number, defined in Eq. (17)
$E_{A,diff}$	activation energy of the diffusivity (J mol^{-1})
E_A^{app}	apparent activation energy for diffusion (J mol^{-1})
F	molar flow rate (mol s^{-1})
i	number
k	reaction rate constant (mol kg_{cat}^{-1} s^{-1} Pa^{-1})
K	adsorption equilibrium constant (Pa^{-1})
K_{eq}	overall reaction equilibrium constant (Pa^{-1})
K_0	pre-exponential of the adsorption equilibrium constant (Pa^{-1})
L_{tube}	permeable membrane length (m)
m_{cat}	catalyst mass (kg)
M	molar mass (g mol^{-1})
N	flux (mol m^{-2} s^{-1})
p	pressure (Pa)
Pe_L, Pe_δ	Péclet number, defined in Eq. (16)
q^{sat}	zeolite saturation loading (mol kg^{-1})
R	gas constant (J mol^{-1} K^{-1})
S	selectivity
STY	Space Time Yield (mol m^{-3} s^{-1})
T	temperature (K)
u	gas velocity
V	volume (m^3)
$WHSV$	Weight Hourly Space Velocity (kg_{feed} kg_{cat}^{-1} h^{-1})
x	space (m); or molar fraction
X	conversion
Y_E	isobutene yield
z	dimensionless tube length (x/L_{tube})
Đ	Maxwell–Stefan diffusivity (m^2 s^{-1})
Đ$_0$	pre-exponential of the Maxwell–Stefan diffusivity (m^2 s^{-1})
$\Re$	reaction rate (mol kg_{cat}^{-1} s^{-1})

Greek letters

α^{ideal}	ideal selectivity, defined in Eq. (22)
α^{mix}	mixture selectivity, defined in Eq. (23)
ΔH_{ads}	adsorption energy (J mol^{-1})
δ^{mem}	membrane thickness (m)
ε	membrane defect porosity
ϑ	dimensionless gas velocity, defined in Eq. (16)
ν	stoichiometric coefficient
ρ	zeolite density (kg m^{-3})
τ	membrane defect tortuosity

Subscripts

A	isobutane
E	isobutene
Ci	hydrocarbon, $i = 1$: methane, $i = 2$: ethane or ethene, etc.
H	hydrogen
i	component
tot	total

Superscripts

conv	convective
diff	diffusive
eff	effective
g	gas
in	ingoing
mem	membrane
out	outgoing
perm	permeate
ret	retentate
S	shell side
T	tube side

Acknowledgements

NGK Insulators is gratefully acknowledged for providing the membrane. Isabelle Aerts and Anna Tihaya are gratefully acknowledged for their contribution to the model development and membrane reactor experiments, respectively.

References

[1] B.M. Weckhuysen, R.A. Schoonheydt, Catalysis Today 51 (1999) 223.
[2] J.A. Moulijn, M. Makkee, A. van Diepen, Chemical Process Technology, Wiley, New York, 2001.
[3] R. Schafer, M. Noack, P. Kolsch, M. Stohr, J. Caro, Catalysis Today 82 (2003) 15.
[4] J. Sanchez, T.T. Tsotsis, Catalytic Membranes and Membrane Reactors, Wiley-VCH, Weinheim, 2002.
[5] D. Casanave, A. Giroir-Fendler, J. Sanchez, R. Loutaty, J.A. Dalmon, Catalysis Today 25 (1995) 309.
[6] D. Casanave, P. Ciavarella, K. Fiaty, J.-A. Dalmon, Chemical Engineering Science 54 (1999) 2807.
[7] P. Ciavarella, D. Casanave, H. Moueddeb, S. Miachon, K. Fiaty, J.-A. Dalmon, Catalysis Today 67 (2001) 177.
[8] U. Illgen, R. Schäfer, M. Noack, P. Kölsch, A. Kühnle, J. Caro, Catalysis Communications 2 (2001) 339.
[9] L. van Dyk, S. Miachon, L. Lorenzen, M. Torres, K. Fiaty, J.-A. Dalmon, Catalysis Today 82 (2003) 167.
[10] W.Q. Liang, R. Hughes, Catalysis Today 104 (2005) 238.
[11] M. Sheintuch, R.M. Dessau, Chemical Engineering Science 51 (1996) 535.
[12] Y.L. Guo, G.Z. Lu, Y.S. Wang, R. Wang, Separation and Purification Technology 32 (2003) 271.
[13] T. Matsuda, I. Koike, N. Kubo, E. Kikuchi, Applied Catalysis A: General 96 (1993) 3.
[14] T. Ioannides, G.R. Gavalas, Journal of Membrane Science 77 (1993) 207.
[15] G. Sznejer, M. Sheintuch, Chemical Engineering Science 59 (2004) 2013.
[16] J.P. Collins, R.W. Schwartz, R. Sehgal, T.L. Ward, C.J. Brinker, G.P. Hagen, C.A. Udovich, Industrial & Engineering Chemistry Research 35 (1996) 4398.
[17] J. van den Bergh, N. Nishiyama, F. Kapteijn, Zeolite membranes in catalysis; what is new and how bright is the future? in: A. Cybulski, J.A. Moulijn, A. Stankiewicz (Eds.), Novel Concepts in Catalysis and Chemical Reactors, Wiley, New York, 2010, p. 211 (Chapter 10).
[18] Y.V. Gokhale, R.D. Noble, J.L. Falconer, Journal of Membrane Science 103 (1995) 235.
[19] W. Zhu, F. Kapteijn, J.A. Moulijn, Chemical Communications 24 (1999) 2453.
[20] J. Gascon, W. Blom, A. van Miltenburg, A. Ferreira, R. Berger, F. Kapteijn, Microporous and Mesoporous Materials 115 (2008) 585.
[21] T. Tomita, K. Nakayama, H. Sakai, Microporous and Mesoporous Materials 68 (2004) 71.
[22] J. van den Bergh, W. Zhu, J. Gascon, J.A. Moulijn, F. Kapteijn, Journal of Membrane Science 316 (2008) 35.
[23] J. van den Bergh, W. Zhu, F. Kapteijn, J.A. Moulijn, K. Yajima, K. Nakayama, T. Tomita, S. Yoshida, Research on Chemical Intermediates 34 (2008) 467.
[24] J. Kuhn, K. Yajima, T. Tomita, J. Gross, F. Kapteijn, Journal of Membrane Science 321 (2008) 344.
[25] J. van den Bergh, A. Tihaya, F. Kapteijn, Microporous and Mesoporous Materials 132 (2010) 137.
[26] S. Himeno, T. Tomita, K. Suzuki, K. Nakayama, K. Yajima, S. Yoshida, Industrial & Engineering Chemistry Research 46 (2007) 6989.
[27] A. Seidel-Morgenstern (Ed.), Membrane Reactors, Wiley, Weinheim, 2010.
[28] F. Kapteijn, W. Zhu, J.A. Moulijn, T.Q. Gardner, Zeolite membranes: modeling and application, in: A. Cybulski, J.A. Moulijn (Eds.), Structured Catalysts and Reactors, Taylor & Francis Group, Boca Raton, FL, 2005, p. 701 (Chapter 20).
[29] J. Happel, K. Kamholz, D. Walsh, V. Strangio, Industrial & Engineering Chemistry Fundamentals 12 (1973) 263.
[30] S. Battersby, P.W. Teixeira, J. Beltramini, M.C. Duke, V. Rudolph, J.C. niz da Costa, Catalysis Today 116 (2006) 12.
[31] Website Athena Visual studio, http://www.athenavisual.com/ (visited 2010).
[32] J.M. van de Graaf, E. van der Bijl, A. Stol, F. Kapteijn, J.A. Moulijn, Industrial & Engineering Chemistry Research 37 (1998) 4071.
[33] W.N. Fueller, P.D. Schettler, J.C. Giddings, Industrial & Engineering Chemistry Research 58 (1966) 19.
[34] S.M.K. Airaksinen, M.E. Harlin, A.O.I. Krause, Industrial & Engineering Chemistry Research 41 (2002) 5619.
[35] J.M. van de Graaf, M. Zwiep, F. Kapteijn, J.A. Moulijn, Applied Catalysis A: General 178 (1999) 225.
[36] H.S. Fogler, Elements of Chemical Reaction Engineering, Pearson Education, New York, 2006.
[37] S.A.S. Rezai, Y. Traa, Journal of Membrane Science 319 (2008) 279.
[38] S. Miachon, J.A. Dalmon, Topics in Catalysis 29 (2004) 59.
[39] R. Dittmeyer, K. Svajda, M. Reif, Topics in Catalysis 29 (2004) 3.